



# $T_1$ Mapping for Myocardial Fibrosis by Cardiac Magnetic Resonance Relaxometry—A Comprehensive Technical Review

Christian R. Hamilton-Craig<sup>1,2\*</sup>, Mark W. Strudwick<sup>3</sup> and Graham J. Galloway<sup>1,4</sup>

<sup>1</sup> Centre for Advanced Imaging, University of Queensland, Brisbane, QLD, Australia, <sup>2</sup> The Prince Charles Hospital, Brisbane, QLD, Australia, <sup>3</sup> Medical Imaging and Radiation Science, Monash University, Clayton, VIC, Australia, <sup>4</sup> Translational Research Institute, Brisbane, QLD, Australia

Cardiac magnetic resonance (CMR) imaging has been widely used to assess myocardial perfusion and scar and is the non-invasive gold standard for identification of focal myocardial fibrosis. However, the late gadolinium enhancement technique is limited in its accuracy for absolute quantification and assessment of diffuse myocardial fibrosis by technical and pathophysiological features. CMR relaxometry, incorporating  $T_1$  mapping, has emerged as an accurate, reproducible, highly sensitive, and quantitative technique for the assessment of diffuse myocardial fibrosis in a number of disease states. We comprehensively review the physics behind CMR relaxometry, the evidence base, and the clinical applications of this emerging technique.

## OPEN ACCESS

### Edited by:

Joseph B. Selvanayagam,  
Flinders University, Australia

### Reviewed by:

Gaetano Nucifora,  
South Australian Health and Medical  
Research Institute, Australia  
Diego Bellavia,  
Istituto Mediterraneo per i Trapianti e  
Terapie ad Alta Specializzazione, Italy

### \*Correspondence:

Christian R. Hamilton-Craig  
c.hamiltoncraig@uq.edu.au

### Specialty section:

This article was submitted to  
Cardiovascular Imaging, a section of  
the journal *Frontiers in Cardiovascular  
Medicine*

**Received:** 10 June 2016

**Accepted:** 24 November 2016

**Published:** 16 March 2017

### Citation:

Hamilton-Craig CR, Strudwick MW  
and Galloway GJ (2017)  $T_1$  Mapping  
for Myocardial Fibrosis by Cardiac  
Magnetic Resonance Relaxometry—A  
Comprehensive Technical Review.  
*Front. Cardiovasc. Med.* 3:49.  
doi: 10.3389/fcvm.2016.00049

**Keywords:**  $T_1$  mapping, cardiac magnetic resonance, MRI, relaxometry, cardiovascular imaging

Cardiac magnetic resonance (CMR) imaging has been used widely to assess myocardial perfusion and scar (1–5). It is the non-invasive gold standard for left and right ventricular quantitation, as well as the assessment and quantitation of focal myocardial fibrosis (after infarction or due to other causes of cellular injury). Myocardial necrosis causes high signal on late gadolinium enhancement (LGE) inversion recovery (IR)  $T_1$ -weighted images with excellent signal-noise ratios, and this has become the reference standard for non-invasive scar imaging in cardiomyopathies of various causes (1–4). However, LGE is limited in its ability to assess and quantitate diffuse (non-focal) myocardial injury and fibrosis. LGE is affected by inconsistencies in acquisition parameters, such as choice inversion time (TI), and in post-processing when signal intensity (SI) thresholds may be arbitrarily applied to distinguish normal myocardium from fibrotic tissue (6, 7). Moreover, the critical issue with LGE is that SI is expressed on an arbitrary scale (*relative SI* compared to “nulled” normal myocardium). Imaging of myocardial fibrosis using *relative* differences between scar and normal myocardium tissue is therefore *qualitative*. Semi-quantitative analysis of LGE can be performed using signal thresholding applied to LGE images; however, there are differences in technique for infarct quantitation (8), and this is only relevant when regional scar/enhancement is present; it does not allow quantitation of diffuse interstitial fibrosis.

Thus, in non-ischemic cardiomyopathies, such as hypertension or diabetes, LGE CMR is unable to detect signal differential where the collagen deposition is diffuse and widespread throughout the myocardium (9).

## CMR RELAXOMETRY

Cardiac magnetic resonance is an evolving technique, providing valuable and comprehensive data on the anatomy and functional integrity of both the heart and coronary blood vessels. Currently,

CMR is performed at magnetic field strengths of 1.5 or 3 T. MR images generate by exploiting the magnetic property (called spin) of nuclei that have an odd atomic number or mass number (10). A proton generates a small magnetic field much like a bar magnet, because the proton has mass, a positive charge, and spins. This small magnetic field is referred to as its magnetic moment. The single proton of the hydrogen molecule gives it a significant magnetic moment and combined with its abundance in the human body, makes it an ideal marker for clinical MRI.

In the absence of an applied magnetic field, the magnetic moments of the hydrogen nuclei are oriented randomly; when placed in a high static magnetic field ( $B_0$ ) they will align either parallel or anti-parallel to the magnetic field. Spins that aligned parallel to  $B_0$  have a lower energy than those aligned anti-parallel, and therefore more align parallel creating a net magnetization ( $M_0$ ) of the sample in the direction of the magnetic field  $B_0$  (11).

## Larmor Equation

The interaction of a magnetic moment with  $B_0$  causes the magnetic moment to precess about the axis of the static magnetic field ( $B_0$ ), at a frequency specific to the strength of ( $B_0$ )— the Larmor frequency. The Larmor frequency is defined as follows:

$$\nu = \frac{\gamma}{2\pi} B_0,$$

where  $\nu$  is the frequency, in megahertz,  $B_0$  is the strength of the magnetic field,  $\gamma$  is the gyromagnetic ratio for hydrogen, and  $\gamma/2\pi = 42.57$  MHz/T (11).

When a radio frequency (RF) pulse at the Larmor frequency is applied to the nuclei within the magnetic field, nuclei begin to resonate and those in the lower energy state absorb energy. Depending on the RF pulse length, the precession of affected nuclei will be moved into the transverse magnetization plane ( $xy$  axis) and be in phase. With cessation of the RF field, the nuclei will realign to their original orientation parallel to  $B_0$ —a process referred to as relaxation. During the relaxation process, the net relaxation induces an RF signal, at the characteristic frequency, which can be measured by a receiver coil. This signal is known as free induction decay (FID).

## MRI Relaxation Time

Three different properties of the interaction of the magnetic moments with  $B_0$  can be measured. These are the longitudinal time constant  $T_1$ , or “spin-lattice” relaxation, and transverse time constant  $T_2$ , or “spin-spin” relaxation and  $T_2^*$ , which is governed by a combination of the effect of spin-spin relaxation, and the homogeneity of the magnetic field. These constants are parameters that are used in MRI to distinguish between normal tissue types and pathological process. The SI of these times depends on the technical parameters that are used for image acquisition (12, 13) and the magnetic properties of a given tissue (14). At a given magnetic field strength, each tissue has a normal range for relaxation time. So, the variation of relaxation time from their normal value can be used to identify pathological process (e.g., edema and scar tissue).

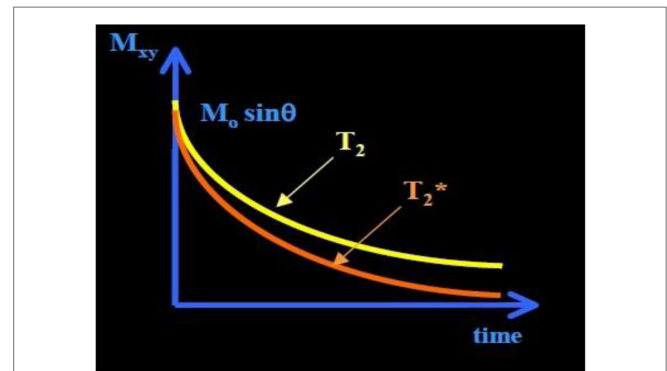


**FIGURE 1 |  $T_2$  and  $T_2^*$  curve.** The  $T_2^*$  has shorter time than  $T_2$  time.  $T_2^*$  exponential decay ( $\approx 30$ – $100$  ms, and shorter for higher  $B_0$ ).

$T_1$  relaxation time refers to the tissue-specific time constant and is a measure of the time taken for protons to realign with the static field after perturbation by the RF pulse. This realignment with  $B_0$  is termed  $T_1$  longitudinal relaxation and the time in milliseconds. The above diagram  $T_1$  recovery curves demonstrate the fat has shorter  $T_1$  times than water molecules. This results from the fact that the fat nuclei lose their energy to lattice quickly, due to slow molecular motion, giving a relatively shorter  $T_1$  time. The quicker the system returns to the equilibrium state, such as occurs in fat, the greater the magnetization available to be excited by the next imaging pulse, producing more signals. Thus, fat appears bright in  $T_1$ -weighted image (11).

$T_2$  relaxation causes decay of signal arising from the dephasing of nuclear precession and consequent loss of net coherence (Figure 1) (15).  $T_2$  decay due to the magnetic interaction that occurs between protons, results in an exponential decay of the transverse magnetization vector, also governed by tissue structure. Unlike  $T_1$  relaxations,  $T_2$  does not involve a transfer of energy but only a change in phase. The water molecules have a long  $T_2$  decay and appear brighter in  $T_2$ -weighted images due to the property that more rapidly moving molecules have a lower tendency to transfer their spin leading to a slower dephasing of the transverse magnetization.

A third decay parameter,  $T_2^*$ , describes the decay of transverse magnetization, due to spin-spin relaxation ( $T_2$ ), together with inhomogeneity in the static magnetic field ( $\Delta B_0$ ), which occurs at tissue interfaces. This leads to a more rapid loss of phase coherence and the MR signal. These relaxation times are influenced by several factors, including field strength, blood iron content, blood volume, temperature, and blood oxygenation (15).

## MYOCARDIAL $T_1$ MAPPING IN THE SETTING OF MYOCARDIAL FIBROSIS

The conventional  $T_1$  mapping method can be generated with an inversion recovery spin echo (IR-SE) sequence. Spin echo uses a  $180^\circ$  RF pulse to invert the spins within the selected slice, followed by a  $90^\circ$  RF pulse rotate the recovered magnetization at TI into the transverse plane, and a further  $180^\circ$  RF pulse to form the spin echo (12). Sampling of IR curve repeats multiple times with

different TIs. The repetition time (TR) of the sequence must be long enough for recovery longitudinal magnetization before the next 180° inversion pulse. The SI of the final image is proportional to the relaxed fraction of the magnetization during the TI as follows:

$$SI = CM_0 \exp\left(-\frac{TE}{T_2}\right) \left[1 - 2 \exp\left(-\frac{TI}{T_1}\right)\right],$$

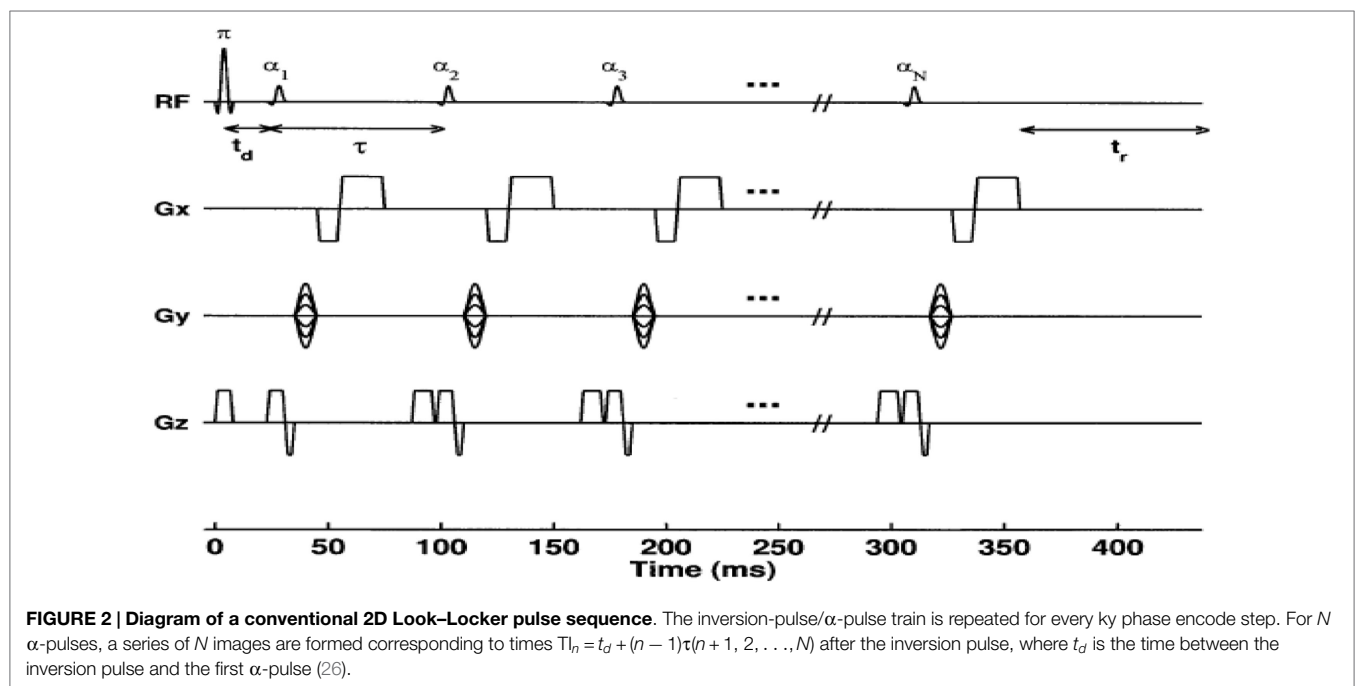
where the first exponential term relates to signal decay due to transverse relaxation (during TE), the second exponential refers to  $T_1$  relaxation (during TI). IR-SE is a gold standard to estimate  $T_1$  with a good accuracy. However, the drawback of IR-SE is that the TR of the sequence should be very long, i.e., TR should be at least five times longer  $T_1$  to allow full recovery of longitudinal magnetization. To reduce the acquisition time, inversion recovery turbo spin echo is currently used for routine clinical purposes (12).

On traditional  $T_1$ -weighted images, the focal differences in  $T_1$  signal are measured qualitatively, assessed by visual inspection using relative units, and cannot be consistently compared between scans (16). For more precise measurement, an emerging technique for CMR  $T_1$  mapping has been applied to measure myocardial signal (in milliseconds) directly on a standardized scale within a single breath hold. This quantification of  $T_1$  mapping provides a benefit over the  $T_1$ -weighted imaging of the myocardium by giving a quantitative measure of  $T_1$  time from multiple scans. A parametric map can be then reconstructed by calculating  $T_1$  values on a pixel-by-pixel basis (17), so, pixel intensities correspond to  $T_1$  values. Different cardiac MR acquisition sequences have been applied to create myocardial  $T_1$  maps, including Look–Locker (LL) and modified Look–Locker inversion recovery (MOLLI) (9, 16, 18–24).

## $T_1$ Mapping Using the LL Technique

The most common technique to measure spin-lattice  $T_1$  relaxation time values is the eponymously named “LL” sequence (also known as “TI scout”). It has been widely used to estimate the optimal TI for assessment of myocardial LGE (23, 25). It was originally proposed by Look and Locker in 1968 and developed more fully in 1970 (24). It consists of an initial inversion pulse, followed by a train of pulses with a constant, limited flip angle (7–15°). The inversion pulse prepares the longitudinal magnetization, which then recovers exponentially according to the  $T_1$  (24). The experiment is repeated until the  $k$ -space Cartesian map of data is filled, allowing an image to be reconstructed. By producing a train of absorption or dispersion signals (continuous wave magnetic resonance) or FIDs (pulsed magnetic resonance), it is possible to save time in spin-lattice relaxation measurements due to the fact that it is not necessary to wait for equilibrium magnetization before initiating the train (24) (see **Figure 2**). The total time required to acquire  $T_1$  would be significantly reduced compared to IR because the LL technique allows for multiple of  $M_z$  in a single measurement period (TM).

It was co-opted by Kaptein et al. in 1976 to quickly sample the recovery after a preparation pulse, during the recovery period or transient phase (27). This method was developed into the T one by multiple readout pulses (TOMROP) imaging sequence (28). In TOMROP, the multiple samples of a particular recovery after RF preparation each correspond to separate image. To acquire a complete data set for each image, the whole sequence must be repeated numerous times. Each repetition fills the next line of  $k$ -space for each image, and so on. Each image has a unique delay time. Early LL-based  $T_1$  techniques required the return to equilibrium of the spin system before the next application of an RF preparation pulse. Consequently, the acquisition time per slice of such implementations was long (28). Hinson and Sobol (29) used



an LL method with no preparation pulse but the method suffered from poor accuracy, attributed to the slice profile. The late 1980s and early 1990s saw the LL method used for  $T_1$  measurements in a number of publications. Crawley and Henkelman (30) compared a number of one-shot and IR methods (LL, saturation recovery, IR, and stimulated echo) and concluded that the LL method was almost as efficient (in terms of dynamic range of the data and the proportion of the imaging time used to sample MR signals) as IR. Brix and colleagues used the TOMROP method with 32 gradient echoes to test for non-exponential behavior, found in fatty tissues (31), in a total acquisition time of 4 min. The LL single-shot IR method has been optimized and refined (32, 33) including improved RF preparation pulses (34, 35).

Echo-planar imaging (EPI) was incorporated into the IR LL-based method (36), by interleaving EPI readouts for eight different slices after an inversion pulse. The sequence was repeated, and the slice order was changed to achieve a range of TIs for each slice, with a total acquisition time of 30 s. LL with EPI was later applied *in vivo* in less than 3 s (37), using a modified blipped EPI technique (38), sacrificing accuracy to some extent. An entire image was acquired at each point on a single recovery of longitudinal magnetization after a saturation pulse. The technique was optimized in 1998 (39) and has found applications in pharmacokinetic modeling (25).

The development of LL technique, which is available on Philips, GE, and Siemens platforms, is summarized in **Table 1**.

The LL sequence has been widely applied in CMR due to its fast acquisition with minimal breath-hold requirements. The LL sequence has been used to measure  $T_1$  values in patients with myocardial fibrosis (23). However, it suffers from significant limitations: low flip angle RF pulse exciting the magnetization and the two RR intervals in the LL sequence are not sufficient for the magnetization to return to equilibrium. This causes *underestimation* of true  $T_1$  values using LL. Furthermore, the LL  $T_1$  images with different TIs are acquired at different cardiac phases. Therefore, images are “cine” with cardiac motion effect, which requires tedious manually tracking of the myocardial borders for each phase, a labor-intensive and error-prone process which will be challenging in clinical practice. The drawing of regions of interest (ROI) in myocardial segments requires adjusting for cardiac motion, which result in including blood pool (partial volume averaging) and artificially increasing the measured  $T_1$  (40).  $T_1$  times between patients may vary due to differences in Gd kinetics (such as in renal impairment), or with different contrast agents; correction factors have been proposed using kinetic modeling for the LL technique (41).

To address these shortcomings, several myocardial  $T_1$  mapping sequences have been created, including MOLLI.

## $T_1$ Mapping with MOLLI

Currently, the most evaluated sequence for myocardium  $T_1$  mapping is an MOLLI sequence (22, 42). The  $T_1$  mapping identifies a significant variation between normal and abnormal myocardium. It demonstrates that the myocardial fibrosis among different myocardial disorders includes ischemia (18), acute/chronic infarction (19), amyloidosis (20), diabetic (21), dilated and hypertrophic cardiomyopathy (17), and heart failure (9).

**TABLE 1 | Summary of development of Look–Locker (LL) technique.**

Reference	Summary of research findings
Look and Locker (24)	Initial proposition of LL technique
Look and Locker (24)	Fully analyzed NMR pulse sequence to measure a spin-lattice $T_1$ relaxation time
Kaptein et al. (27)	LL was co-opted to quickly sample the recovery after a preparation pulse during the recovery period
Gerumann (28)	T one by multiple readout pulses (TOMROP) was proposed in which the multiple samples of a particular recovery after radio frequency (RF) preparation each corresponds to separate image
Hinson and Sobol (29)	LL method was applied without preparation pulse
Crawley and Henkelman (30)	Compared [LL, saturation recovery, inversion recovery (IR), and stimulated echo] and concluded that LL was almost as efficient
Brix et al. (31)	TOMROP was used with 32 gradient echoes in a total acquisition time of 4 min
Kay and Henkelman (32)	LL single-shot IR method has been optimized and refined
Gowland and Leach (33)	LL single-shot IR method has been optimized and refined
Been et al. (34)	Improved RF preparation pulses
Gowland et al. (35)	Improved RF preparation pulses
Ordidge et al. (36)	Echo-planar imaging (EPI) was incorporated into the IR LL-based method
Gowland and Mansfield (37)	EPI was applied <i>in vivo</i> in less than 3 s
Freeman et al. (39)	An entire image was acquired at each point on a single recovery of longitudinal magnetization after a saturation pulse
Karlsson and Nordell (25)	EPI with LL method has found application in pharmacokinetic modeling in the head
Daniel et al. (40)	Modified Look–Locker inversion recovery (MOLLI) is proposed to overcome the limitations of the conventional LL approach for cardiac applications
Daniel et al. (22)	Studied the single breath-hold myocardial MR $T_1$ mapping with MOLLI technique with high spatial resolution at 1.5 T MR reproducibility study
Daniel et al. (58)	Investigated optimization and validation of a fully integrated pulse sequence for (MOLLI) $T_1$ mapping of the heart
lies et al. (9)	Evaluation of diffuse myocardial fibrosis in heart failure with cardiac magnetic resonance contrast-enhanced $T_1$ mapping

Modified Look–Locker inversion recovery is a CMR pulse sequence that is used for accurate  $T_1$  mapping of myocardium with high spatial resolution. A  $T_1$  map of the myocardium is a reconstructed image, where the  $T_1$  relaxation value is computed for every pixel of the corresponding myocardial voxel. Signal recovery from each myocardial voxel is acquired at different TIs following a single inversion pulse, all gated to the same cardiac phase, thereby enabling a pixel-based  $T_1$  quantification in the myocardium. MOLLI has introduced two variations to the standard LL sequence; selective data acquisition at a given time of the cardiac cycle over successive heartbeats, and merging of

image sets from multiple LL experiments with varying TIs into one data set (22, 40). While selective data acquisition effectively decreases the number of images acquired in each LL experiment to one per heartbeat, the use of multiple LL experiments with different TIs increases the number of samples of the relaxation curve to a value that is sufficiently high for accurate  $T_1$  estimation.

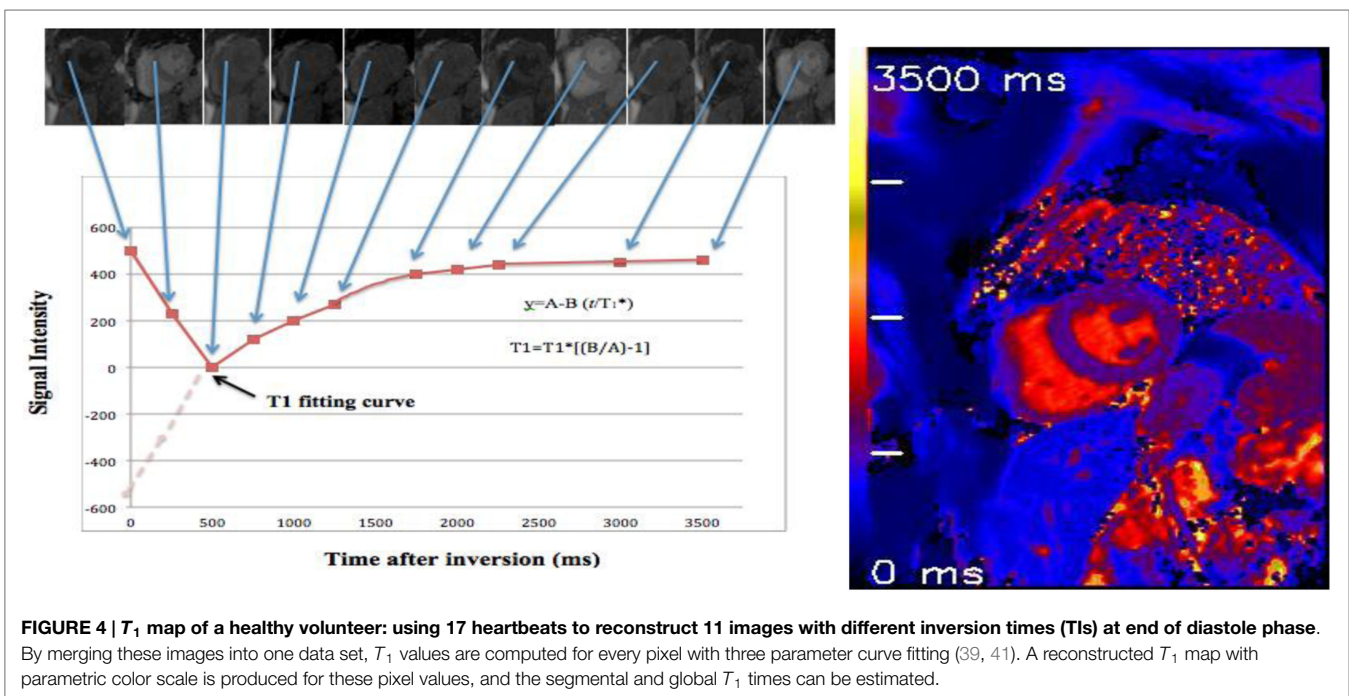
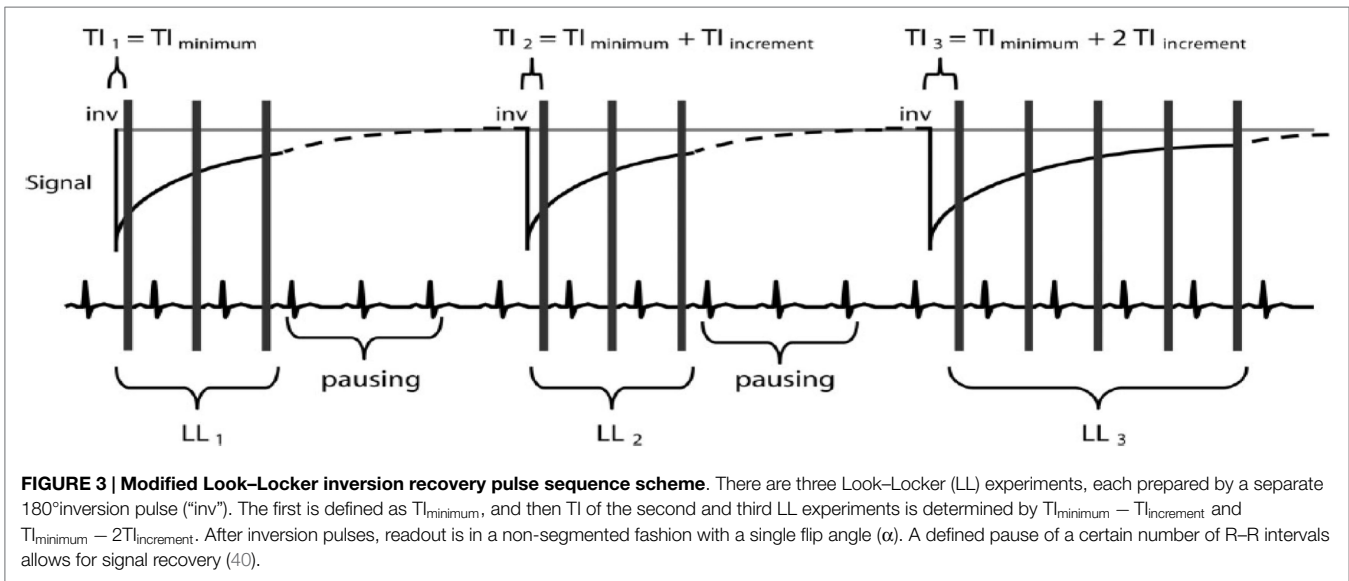
Modified Look-Locker inversion recovery is an ECG-gated pulse sequence scheme and uses three prepared LL experiments consecutively within one breath hold over 17 heartbeats to reconstruct 11 images with different TIs. Three successive ECG-triggered LL experiments (LL<sub>1</sub>, LL<sub>2</sub>, and LL<sub>3</sub>) are carried out with three, three, and five single-shot readouts, respectively, at

end diastole of consecutive heartbeats to sample the recovery of longitudinal magnetization after the inversion pulse. MOLLI pulse sequence scheme is illustrated (Figure 3).  $T_1$  maps can be generated any time before or after contrast agent (e.g., gadolinium) administration (40).

Reconstruction of  $T_1$  maps from MOLLI source images is performed offline using purpose written customized software, or inline using vendor-specific processing, with ROI (septal or endo-epicardial) able to be analyzed in a pixel-wise quantitative fashion (Figure 4).

Image data are sorted by their effective TI, which are given by

$$t = \text{TI} + (n - 1) \text{RR},$$



where  $N$  = image number within the LL experiment and  $RR$  = heartbeat interval. Three-parameter non-linear curve fitting using a Levenberg–Marquardt algorithm is performed for corresponding pixel, which is given by

$$y = A - B \exp\left(-\frac{t}{T_1^*}\right),$$

where  $y$  denotes SI and  $T_1^*$  corresponds to the apparent, modified  $T_1$  in an LL experiment.

Correction for readout-induced attenuation of the relaxation curve is attempted by using the three-curve fitting parameters  $T_1^*$ ,  $A$ , and  $B$  for the calculation of  $T_1$ . Then,  $T_1$  estimates as in conventional LL methods by

$$T_1 = T_1^* \left( \frac{B}{A} - 1 \right),$$

The MOLLI sequence has been fully described, optimized, tested/re-tested, in phantoms and in large cohorts of healthy volunteers (22, 40) as well as being applied in cardiomyopathies (9, 17, 18, 20, 43). In addition, the  $T_1$  mapping with MOLLI has been validated against histopathology for assessment of myocardial fibrosis. It demonstrated that the pre-contrast “native  $T_1$ ” has a linear correlation with percentage of myocardial fibrosis as measured histologically on invasive myocardial biopsy.  $T_1$  times post-contrast administration (10–15 min) had an inverse linear relationship with collagen content in myocardial fibrosis subjects (9, 44, 45).

Nacif et al. (46) compared  $n = 168$  myocardial  $T_1$  maps using LL and MOLLI at 1.5 T, showing that pre-contrast (native)  $T_1$  values had good agreement, but LL had wider limits of agreement, and post-contrast  $T_1$  maps also had good agreement but with LL giving higher values than MOLLI, hence they are not interchangeable (46).

$T_1$  mapping can be generated for different segments of the myocardium (base, mid-cavity, and apex) within a single breath

hold of about 15–20 s. However, the apex  $T_1$  values with MOLLI are slightly higher than basal and mid-cavity. The increasing in  $T_1$  values may be caused by partial volume effect and some degree of overestimation effect in apical level of left ventricle. These effects occur as a result of the ventricular wall being somewhat tilted toward the apex and no longer being aligned perpendicular to the short axis images (47–49).

Furthermore,  $T_1$  mapping with MOLLI has a greater reproducibility, accuracy, and an excellent overall inter- and intraobserver agreement over a wide range of TIs in pre- and post-contrast agent administration compared to the LL technique (22, 42). However, the  $T_1$  mapping with MOLLI sequence is sensitive to extremes of heart rate (bradycardia or tachycardia) (22) leading to slightly underestimation of  $T_1$  values. This may be corrected though “heart rate correction” by changing in the timing of the readouts with respect to the inversion pulses at different heart rates. This variation introduces various degrees of disturbance of the  $T_1$  relaxation curve. The heart rate affects the  $T_1$  value if the  $T_1$  value is higher than 750 ms or less than 200 ms with MOLLI (22, 42).

Moreover, MOLLI is limited by long breath hold about 15–20 s (17 heart beats to acquire the final  $T_1$  maps). This may be difficult for elderly and pulmonary compromised patients and generates respiratory and motion artifacts (50). However, modern inline processing provides registration tools to reduce motion artifacts before the computation of final  $T_1$  maps (motion corrected or “MoCo MOLLI”). This will minimize the sensitivity of  $T_1$  mapping to motion artifacts and heart rate. Also, various acquisition sequences with short breath hold, such as shortened modified Look–Locker inversion recovery, have been validated and recently applied for cardiomyopathies (51, 52). At 1.5 T, the pre- and post-contrast (10 min)  $T_1$  times of normal myocardium are  $980 \pm 53$  and  $470 \pm 26$  ms, respectively (Figure 5) (22). Pre-contrast  $T_1$  values of myocardial fibrosis (infarction scar) are significantly longer than those of normal myocardium ( $1,060 \pm 61$  vs.  $987 \pm 34$  ms) (43). The longer pre-contrast  $T_1$  values in myocardial fibrosis patients have been reported in different cardiomyopathies.

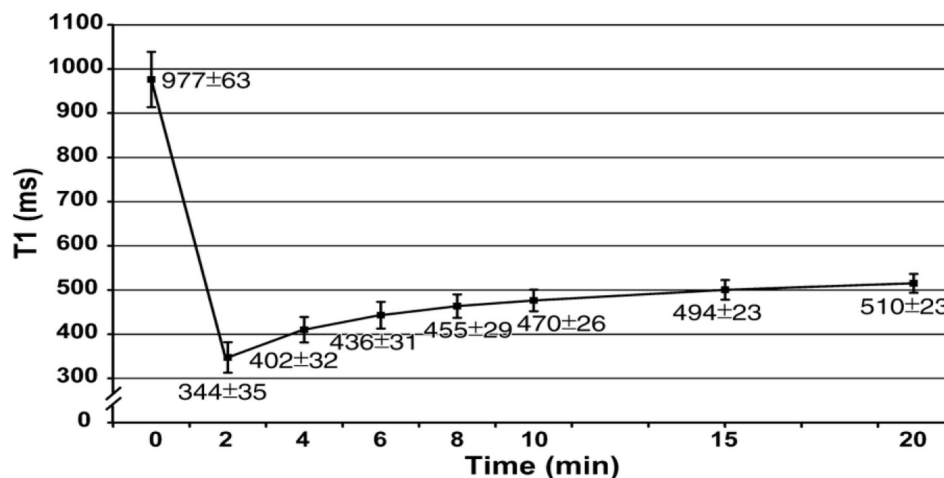


**FIGURE 5 |** Graph shows recovery of absolute  $T_1$  (mean  $\pm$  SD in milliseconds) at 1.5 T in mid-cavity short axis slices at pre- and post-contrast (0–20 min) after administration of 0.15 mmol/kg of gadopentetate dimeglumine (22).

Infarction, myocarditis, and interstitial diffuse fibrosis, all have high pre-contrast  $T_1$  values when compared with normal myocardial  $T_1$  times (17, 20, 43). However, longer  $T_1$  values may also be noticed in different pathologically important processes, such as edema (53). Previous phantom, animal, and human tissue based studies lend insight into the effects on  $T_1$  signal by showing that  $T_1$  increases with increased water content and amount of extracellular fibrillar macromolecules (14, 54). Messroghli et al. concluded that increased myocardial  $T_1$  mapping corresponds to the areas of the human myocardial infarction, which showed on LGE (43). However, the links between the exact molecular mechanism in healthy tissue and myocardial fibrosis and corresponding pre-contrast  $T_1$  are less well understood. On the hand, the decrease in post-contrast  $T_1$  values in diffuse myocardial fibrosis has been previously related to increased extracellular space. It has been well described in acute, chronic ischemic, diffuse myocardial fibrosis, and inflammatory myocardial injury. The post-contrast  $T_1$  times (10 min) were significantly shorter in chronic infarct scar compared with normal myocardium at 0.15 mmol/kg ( $390 \pm 20$  vs.  $483 \pm 23$  ms, respectively) (43).

Also,  $T_1$  mapping with high magnetic field (3 T) has been reported in a few studies of interstitial myocardial fibrosis. It was similar to 1.5 T, the pre-contrast  $T_1$  was longer, and post-contrast  $T_1$  was shorter in myocardial fibrosis patients compared to normal myocardium. Puntmann et al. (55) reported higher pre-contrast  $T_1$  values for hypertrophic and non-ischemic-dilated cardiomyopathies at 3 T compared to controls (hypertrophic  $1.254 \pm 43$  ms and non-ischemic-dilated cardiomyopathy  $1.239 \pm 57$  ms vs. healthy  $1.070 \pm 55$  ms). Also, the post-contrast  $T_1$  values (10 min) at 3 T were shorter in hypertrophic and dilated cardiomyopathies compared to healthy (hypertrophic:  $307 \pm 47$  ms, dilated cardiomyopathies:  $296 \pm 43$  ms vs. controls:  $402 \pm 58$  ms) (55).

There are studies published for normal and diffuse myocardial fibrosis of myocardium  $T_1$  values, as described comprehensively in **Tables 2** and **3**.

The myocardium is made of densely packed myocytes, contributing to approximately 90% of myocardial mass. Signal from pre-contrast imaging reflects the majority of signal from the myocytes themselves. Conversely, in post-contrast imaging, the majority of Gd-based contrast signal arises from the interstitium (as Gd is an extracellular contrast agent and does not, therefore, reside within myocytes unless they are damaged); thus, post-contrast  $T_1$  mainly reflects interstitial or replacement fibrosis (see **Box 1**, below), hence the ability to calculate extracellular volume (ECV) from the difference between these two parameters.

## Extracellular Volume

$T_1$  mapping data can be used to calculate ECV fraction, using the pre- and post-contrast  $T_1$  times and hematocrit. Details of this technique and its uses are beyond the scope of this review; SCMR guidelines exist to guide application of  $T_1$  mapping and ECV quantitation (65).

## Limitations of $T_1$ Mapping

Challenges remain with myocardial relaxometry for  $T_1$  mapping. These include technical challenges such as variations of  $T_1$  times at different field strength and across different vendors, and the

**TABLE 2 | Healthy clinical studies using  $T_1$  and  $T_2^*$ .**

Reference	Sample size	$T_1/T_2^*$ mapping sequence	Result of $T_1$ or $T_2^*$ mapping (ms)
Wacker et al. (56)	5	srTFL, segmented $T_2^*$ gradient echo pulse	$T_1 = 1,219 \pm 72$ ms $T_2^* = 35 \pm 3$ ms
Sebastian et al. (57)	12	LL	$T_1 = 1,033 \pm 126$ ms $T_2^* = \text{NA}$
Messroghli et al. (22)	15	MOLLI	$T_1 = 980 \pm 53$ ms $T_2^* = \text{NA}$
Messroghli et al. (58)	20	MOLLI	$T_1 = 939 \pm 63$ ms $T_2^* = \text{NA}$
Sparrow et al. (59)	15	MOLLI	$T_1 = 980 \pm 53$ ms $T_2^* = \text{NA}$
Iles et al. (9)	20	VAST	$T_1 = 975 \pm 62$ ms $T_2^* = \text{NA}$
Li et al. (60)	13	2 echo times GRE	$T_1 = \text{NA}$ $T_2^* = 33 \pm 6.5$ ms
Reeder et al. (61)	5	Multi-echo GRE	$T_1 = \text{NA}$ $T_2^* = 38 \pm 6$ ms
Anderson et al. (62)	15	Multi-echo GRE	$T_1 = \text{NA}$ $T_2^* = 5,216$ ms
Positano et al. (63)	15	Multi-echo GRE	$T_1 = \text{NA}$ $T_2^* = 38.9.2$ ms in endocardial sectors and $33.1 \pm 8.4$ ms in epicardial sectors
Messroghli et al. (64)	20	Multi-echo GRE	$T_1 = \text{NA}$ $T_2^* = 27.9.3.4$ ms in anteroseptal and $23.1 \pm 5.2$ ms in inferolateral
Piechnik et al. (51)	342	shMOLLI	$T_1 = 962.25$ ms $T_2^* = \text{NA}$ Heart rate only physiologic factors effect on myocardial $T_1$ values

NA, not applicable; srTFL, saturation recovery turboFLASH; LL, Lock-Locker; MOLLI, modified Lock-Locker inversion recovery sequence; VAST, inversion recovery gradient echo sequence with variable sampling of the k-space in time; GRE, gradient pulse sequence; shMOLLI, short modified Lock-Locker sequence.

rapidity in growth of pulse sequences being released as product and as works-in-progress, calling into question both the inherent accuracy and the level agreement between these techniques. Furthermore, the variations in  $T_1$  relaxometry values with different contrast doses and image timing require further investigation, to establish the test–retest and inter-site reproducibility of this technique. Next, the challenges to application of  $T_1$  mapping to clinical practice include establishment of robust normal ranges in large cohorts across multiple ethnic groups, and the observation that  $T_1$  mapping appears to be a highly sensitive technique, with the ability to discriminate healthy normal myocardium and identify very early changes in substrate. However, this technique lacks specificity; a wide variety of conditions prolongs native  $T_1$  and/or shortens post-contrast myocardial  $T_1$ . Therefore, further clinical data are required in order to establish the use of these parameters in relation to disease (e.g., early detection of target organ damage in systemic conditions such as hypertension or diabetes), to inform treatment decisions, and their ability to predict or alter clinical outcomes.

**TABLE 3 | Clinical studies using  $T_1$  mapping for myocardial diffuse fibrosis in clinical patients.**

Reference	Cardiac disease category	Patient sample size	$T_1$ mapping method	Summary of findings
Thuny et al. (66)	Systemic sclerosis	37	Modified Look–Locker inversion recovery (MOLLI)	LV diastolic dysfunction had a shorter 15 min post-contrast $T_1$ time (ms) than those with a normal diastolic function ( $431 \pm 7$ vs. $464 \pm 8$ , $p = 0.01$ )
Thibault et al. (67)	Type II diabetic patient	24	MOLLI	Mean myocardial $T_1$ relaxation time was significantly shorter in diabetic patients than in volunteers both at 5 ( $312 \pm 5$ vs. $361 \pm 6$ ms, respectively, $p < 0.001$ ) and 15 min ( $405 \pm 6$ vs. $456 \pm 5$ ms, respectively, $p < 0.001$ ) after gadolinium injection
Ellims et al. (68)	Hypertrophy cardiomyopathy	51	VAST	Post-contrast myocardial $T_1$ time was significantly shorter in patients with HCM compared to controls, consistent with diffuse myocardial fibrosis ( $498 \pm 80$ vs. $561 \pm 47$ ms, $p < 0.001$ )
Kammerlander et al. (69)	Patients with NH <sub>2</sub> -terminal portion of the precursor of brain natriuretic peptide (NT-proBNP)	37	N/A	In patients with NT-proBNP levels $>400$ pg/ml mean $T_1$ was significantly shorter than in patients with NT-proBNP $<400$ pg/ml ( $374.6 \pm 51.1$ vs. $404.6 \pm 34.4$ ms, $p = 0.042$ ) and controls ( $509.4 \pm 46.5$ ms, $p < 0.001$ )
Sibley et al. (70)	Non-ischemic cardiomyopathy	73	Look–Locker (LL)	47 patients had a focal myocardial scar and 26 without scar tissue. The midwall circumferential strain (Ecc) was reduced ( $-13.0 \pm 5.4\%$ ), and mean $T_1$ time was $478 \pm 70$ ms in patients with no scar tissue
Jellis et al. (21)	Type II diabetic patients	67	VAST	Subjects have a shorter post-contrast $T_1 = 434 \pm 20$ ms. Post-contrast $T_1$ was associated with echocardiography diastolic dysfunction (Em $r = 0.28$ , $p = 0.020$ ; E/Em $r = -0.24$ , $p = 0.049$ )
Messroghli et al. (42)	Acute myocardial infarction	8	Inversion recovery (IR)-prepared fast gradient echo sequence	$T_1$ pre-contrast value of the infarcted myocardium was significantly prolonged compared with non-infarcted normal myocardium ( $+18 \pm 7\%$ ). $T_1$ 10-min post-contrast value of the infarct was significantly reduced compared with normal myocardium ( $-27 \pm 4\%$ )
Messroghli et al. (43)	Acute and chronic myocardial infarction	24	MOLLI	In chronic MI, the pre-contrast $T_1$ relaxation time of hyper-enhanced areas was higher than $T_1$ of remote areas ( $1,060 \pm 61$ vs. $987 \pm 34$ ms, $p < 0.0001$ ). In acute MI, the pre-contrast $T_1$ value of hyper-enhanced areas was higher than remote areas ( $1,197 \pm 76$ vs. $1,011 \pm 66$ ). The hyper-enhanced in acute is higher than chronic infarction
Sebastian et al. (57)	Acute and chronic myocardial infarction	10	LL	Mean $T_1$ values of the normal myocardium post-contrast was $536 \pm 66$ ms; chronically infarcted pre-contrast and post-contrast was $1,000 \pm 67$ and $408 \pm 43$ ms, respectively
Sparrow et al. (59)	Myocardial fibrosis in chronic aortic regurgitation	8	MOLLI	There is a significant difference in segmental averaged $T_1$ relaxation between in abnormal wall motion vs. normal control segments in 10, 15, and 20 min after administration, Gd: $510$ vs. $476$ , $532$ vs. $501$ , and $560$ vs. $516$ ms, respectively
Iles et al. (9)	Chronic heart failure	25	VAST	Post-contrast myocardial $T_1$ times were shorter in heart failure subjects than controls ( $383 \pm 17$ vs. $564 \pm 23$ ms) controls even when excluding areas of regional fibrosis. $T_1$ 15-min post-contrast values correlated significantly with collagen volume fraction on myocardial biopsies ( $R = -0.7$ )
Maceira et al. (71)	Cardiac amyloidosis	22	Segmented IR sequence	Subendocardial $T_1$ in amyloid patients was shorter than in controls (at 4 min: $427 \pm 73$ vs. $579 \pm 75$ ms; $p < 0.01$ )

**BOX 1 | Source of T<sub>1</sub> signal.**

Pre-contrast "Native" T<sub>1</sub> = predominant signal from *myocytes* (replacement fibrosis, or intracellular accumulation, e.g., Fabry disease).

Post-contrast T<sub>1</sub> = predominant signal from *interstitial* space (interstitial fibrosis).

**CONCLUSION**

Myocardial T<sub>1</sub> mapping using quantitative relaxometry is an emerging and important tool in the assessment of global myocardial fibrosis. It is a highly sensitive marker of disease but is not specific, with changes in myocardial T<sub>1</sub> occurring in many different conditions. Nevertheless, the high sensitivity and excellent reproducibility of the technique offers a tool for the early detection of myocardial damage, over-and-above techniques such as the CMR LGE technique and other modalities such as speckle tracking echocardiography, pulse wave velocity, and tissue tagging. Native T<sub>1</sub> mapping is proving to be a robust indicator of early myocardial disease in many conditions, and normal ranges and guidelines for post-processing have been published by the Society of Cardiovascular Magnetic Resonance (65). Myocardial T<sub>1</sub> mapping is a rapidly evolving technique, now with longitudinal prognostic data emerging, and normal ranges established at 1.5

**REFERENCES**

- Croisille P, Revel D, Saeed M. Contrast agents and cardiac MR imaging of myocardial ischemia: from bench to bedside. *Eur Radiol* (2006) 16:1951–63. doi:10.1007/s00330-006-0244-z
- Judd RM, Atalay MK, Rottman GA, Zerhouni EA. Effects of myocardial water exchange on T1 enhancement during bolus administration of MR contrast agents. *Magn Reson Med* (1995) 33:215–23. doi:10.1002/mrm.1910330211
- Lima JAC. Myocardial viability assessment by contrast-enhanced magnetic resonance imaging. *J Am Coll Cardiol* (2003) 42:902–4. doi:10.1016/S0735-1097(03)00839-8
- Kim RJ, Chen E-L, Lima JA, Judd RM. Myocardial Gd-DTPA kinetics determine MRI contrast enhancement and reflect the extent and severity of myocardial injury after acute reperfused infarction. *Circulation* (1996) 94:3318–26. doi:10.1161/01.CIR.94.12.3318
- Mahrholdt H, Wagner A, Judd RM, Sechtem U, Kim RJ. Delayed enhancement cardiovascular magnetic resonance assessment of non-ischaemic cardiomyopathies. *Eur Heart J* (2005) 26:1461–74. doi:10.1093/eurheartj/ehi258
- Simonetti OP, Kim RJ, Fieno DS, Hillenbrand HB, Wu E, Bundy JM, et al. An improved MR imaging technique for the visualization of myocardial infarction. *Radiology* (2001) 218:215–23. doi:10.1148/radiology.218.1.r01ja50215
- Spiewak M, Malek LA, Misko J, Chojnowska L, Milosz B, Klopotoski M, et al. Comparison of different quantification methods of late gadolinium enhancement in patients with hypertrophic cardiomyopathy. *Eur J Radiol* (2010) 74:e149–53. doi:10.1016/j.ejrad.2009.05.035
- Flett AS, Hasleton J, Cook C, Hausenloy D, Quarta G, Ariti C, et al. Evaluation of techniques for the quantification of myocardial scar of differing etiology using cardiac magnetic resonance. *JACC Cardiovasc Imaging* (2011) 4:150–6. doi:10.1016/j.jcmg.2010.11.015
- Iles L, Pfluger H, Phrommintikul A, Cherayath J, Aksit P, Gupta SN, et al. Evaluation of diffuse myocardial fibrosis in heart failure with cardiac magnetic resonance contrast-enhanced T1 mapping. *J Am Coll Cardiol* (2008) 52:1574–80. doi:10.1016/j.jacc.2008.06.049
- Matthews PM, Adcock J, Chen Y-P, Fu S, Devlin JT, Rushworth MFS, et al. Towards understanding language organization in the brain using fMRI. *Hum Brain Mapp* (2003) 18:239–47. doi:10.1002/hbm.10099
- Catherine Westbrook CR, John T. *MRI in Practice*. Malden, MA: Blackwell Pub (2005). 44 p.

and 3.0 T in healthy humans and in aging. Further questions remain as to the standardization of pulse sequences across field strengths and between vendors, the affect of contrast type, dose and timing, the post-processing software, and the interpretation of T<sub>1</sub> mapping results to inform clinical practice.

**AUTHOR CONTRIBUTIONS**

CH-C, MS, and GG: main contributions to the conception or design of the work; the interpretation of data for the work; drafted the work and revised it critically for important intellectual content; final approval of the version to be published; and agreement to be accountable for all aspects of the work in ensuring that questions related to the accuracy or integrity of any part of the work are appropriately investigated and resolved.

**ACKNOWLEDGMENTS**

The authors thank Dr. Qurain Alshammari for his input.

**FUNDING**

CH-C was funded by the DSITIA Smart Futures Fellowship Early Careers Grant.

- Kaldoudi E, Williams SCR. Relaxation time measurements in NMR imaging. Part I: longitudinal relaxation time. *Concepts Magn Reson* (1993) 5:217–42. doi:10.1002/cmr.1820050303
- Kingsley PB. Methods of measuring spin-lattice (T1) relaxation times: an annotated bibliography. *Concepts Magn Reson* (1999) 11:243–76. doi:10.1002/(SICI)1099-0534(1999)11:4<243::AID-CMR5>3.3.CO;2-3
- Bottomley PA, Foster TH, Argersinger RE, Pfeifer LM. A review of normal tissue hydrogen NMR relaxation times and relaxation mechanisms from 1-100 MHz: dependence on tissue type, NMR frequency, temperature, species, excision, and age. *Med Phys* (1984) 11:425–48. doi:10.1118/1.595535
- Hasemi RH, Bradley WG, Lisanti CJ. *MRI: The Basics*. Philadelphia: Lippincott Williams & Wilkins (2004).
- Higgins DM, Ridgway JP, Radjenovic A, Sivananthan UM, Smith MA. T1 measurement using a short acquisition period for quantitative cardiac applications. *Med Phys* (2005) 32:1738–46. doi:10.1118/1.1921668
- Dass S, Suttie JJ, Piechnik SK, Ferreira VM, Holloway CJ, Banerjee R, et al. Myocardial tissue characterization using magnetic resonance non-contrast T1 mapping in hypertrophic and dilated cardiomyopathy. *Circ Cardiovasc Imaging* (2012) 5(6):726–33.
- Goldfarb JW, Arnold S, Han J. Recent myocardial infarction: assessment with unenhanced T1-weighted MR imaging. *Radiology* (2007) 245:245–50. doi:10.1148/radiol.2451061590
- Messroghli DR, Greiser A, Fröhlich M, Dietz R, Schulz-Menger J. Optimization and validation of a fully-integrated pulse sequence for modified Look-Locker inversion-recovery (MOLLI) T1 mapping of the heart. *J Magn Reson Imaging* (2007) 26:1081–6. doi:10.1002/jmri.21119
- Karamitsos TD, Piechnik SK, Banypersad SM, Fontana M, Ntusi NB, Ferreira VM, et al. Noncontrast T1 mapping for the diagnosis of cardiac amyloidosis. *JACC Cardiovasc Imaging* (2013) 6:488–97. doi:10.1016/j.jcmg.2012.11.013
- Jellis C, Wright J, Kennedy D, Sacre J, Jenkins C, Haluska B, et al. Association of imaging markers of myocardial fibrosis with metabolic and functional disturbances in early diabetic cardiomyopathy. *Circ Cardiovasc Imaging* (2011) 4:693–702. doi:10.1161/CIRCIMAGING.111.963587
- Messroghli DR, Plein S, Higgins DM, Walters K, Jones TR, Ridgway JP, et al. Human myocardium: single-breath-hold MR T1 mapping with high spatial resolution—reproducibility study. *Radiology* (2006) 238:1004–12. doi:10.1148/radiol.2382041903

23. Amano Y, Takayama M, Kumita S. Contrast-enhanced myocardial T1-weighted scout (Look-Locker) imaging for the detection of myocardial damages in hypertrophic cardiomyopathy. *J Magn Reson Imaging* (2009) 30:778–84. doi:10.1002/jmri.21921
24. Look DC, Locker DR. Time saving in measurement of NMR and EPR relaxation times. *Rev Sci Instrum* (1970) 41:250–1. doi:10.1063/1.1684482
25. Karlsson M, Nordell B. Analysis of the Look-Locker T1 mapping sequence in dynamic contrast uptake studies: simulation and in vivo validation. *Magn Reson Imaging* (2000) 18:947–54. doi:10.1016/S0730-725X(00)00193-4
26. Henderson E, McKinnon G, Lee T-Y, Rutt BK. A fast 3D Look-Locker method for volumetric T1 mapping. *Magn Reson Imaging* (1999) 17:1163–71. doi:10.1016/S0730-725X(99)00025-9
27. Kaptein R, Dijkstra K, Tarr CE. A single-scan Fourier transform method for measuring spin-lattice relaxation times. *J Magn Reson* (1969) 1976(24): 295–300.
28. Graumann R, Barfuss H, Fischer H, Hentschel D, Oppelt A. TOMROP: a sequence for determining the longitudinal relaxation time T1 in NMR. *Electromedica* (1987) 55:67–72.
29. Hinson WH, Sobol WT. A new method of computing spin-lattice relaxation maps in magnetic resonance imaging using fast scanning protocols. *Med Phys* (1988) 15:551–61. doi:10.1118/1.596206
30. Crawley AP, Henkelman RM. A comparison of one-shot and recovery methods in T1 imaging. *Magn Reson Med* (1988) 7:23–34. doi:10.1002/mrm.1910070104
31. Brix G, Schad LR, Deimling M, Lorenz WJ. Fast and precise T1 imaging using a TOMROP sequence. *Magn Reson Imaging* (1990) 8:351–6. doi:10.1016/0730-725X(90)90041-Y
32. Kay I, Henkelman RM. Practical implementation and optimization of one-shot T1 imaging. *Magn Reson Med* (1991) 22:414–24. doi:10.1002/mrm.1910220249
33. Gowland PA, Leach MO. Fast and accurate measurements of T1 using a multi-readout single inversion-recovery sequence. *Magn Reson Med* (1992) 26:79–88. doi:10.1002/mrm.1910260109
34. Been M, Smith MA, Ridgway JP, Douglas RH, de Bono DP, Best JJ, et al. Serial changes in the T1 magnetic relaxation parameter after myocardial infarction in man. *Br Heart J* (1988):1–8. doi:10.1136/hrt.59.1.1
35. Gowland PA, Leach MO, Sharp JC. The use of an improved inversion pulse with the Spin-Echo/inversion-recovery sequence to give increased accuracy and reduced imaging time for T1 measurements. *Magn Reson Med* (1989) 12:261–7. doi:10.1002/mrm.1910120215
36. Ordidge RJ, Gibbs P, Chapman B, Stehling MK, Mansfield P. High-speed multislice T1 mapping using inversion-recovery echo-planar imaging. *Magn Reson Med* (1990) 16:238–45. doi:10.1002/mrm.1910160205
37. Gowland P, Mansfield P. Accurate measurement of T1 in less than 3 seconds using echo-planar imaging. *Magn Reson Med* (1993) 30:351–4. doi:10.1002/mrm.1910300312
38. Ordidge RJ, Howseman A, Coxon R, Turner R, Chapman B, Glover P, et al. Snapshot imaging at 0.5 t using echo-planar techniques. *Magn Reson Med* (1989) 10:227–40. doi:10.1002/mrm.1910100207
39. Freeman AJ, Gowland PA, Mansfield P. Optimization of the ultrafast Look-Locker echo-planar imaging T1 mapping sequence. *Magn Reson Imaging* (1998) 16:765–72. doi:10.1016/S0730-725X(98)00011-3
40. Messroghli DR, Radjenovic A, Kozerke S, Higgins DM, Sivananthan MU, Ridgway JP. Modified Look-Locker inversion recovery (MOLLI) for high-resolution T1 mapping of the heart. *Magn Reson Med* (2004) 52:141–6. doi:10.1002/mrm.20110
41. Gai N, Turkbey EB, Nazarian S, van der Geest RJ, Liu CY, Lima JA, et al. T1 mapping of the gadolinium-enhanced myocardium: adjustment for factors affecting interpatient comparison. *Magn Reson Med* (2011) 65:1407–15. doi:10.1002/mrm.22716
42. Messroghli DR, Niendorf T, Schulz-Menger J, Dietz R, Friedrich MG. T1 mapping in patients with acute myocardial infarction. *J Cardiovasc Magn Reson* (2003) 5:353–9. doi:10.1081/JCMR-120019418
43. Messroghli DR, Walters K, Plein S, Sparrow P, Friedrich MG, Ridgway JP, et al. Myocardial T1 mapping: application to patients with acute and chronic myocardial infarction. *Magn Reson Med* (2007) 58:34–40. doi:10.1002/mrm.21272
44. Sibley CT, Noureldin RA, Gai N, Nacif MS, Liu S, Turkbey EB, et al. T1 mapping in cardiomyopathy at cardiac MR: comparison with endomyocardial biopsy. *Radiology* (2012) 256:724–32. doi:10.1148/radiol.12112721
45. Bull S, White SK, Piechnik SK, Flett AS, Ferreira VM, Loudon M, et al. Human non-contrast T1 values and correlation with histology in diffuse fibrosis. *Heart* (2013) 99:923–7. doi:10.1136/heartjnl-2012-303052
46. Nacif MS, Turkbey EB, Gai N, Nazarian S, van der Geest RJ, Noureldin RA, et al. Myocardial T1 mapping with MRI: comparison of Look-Locker and MOLLI sequences. *J Magn Reson Imaging* (2011) 34:1367–73. doi:10.1002/jmri.22753
47. Lima JA, Jeremy R, Guier W, Bouton S, Zerhouni EA, McVeigh E, et al. Accurate systolic wall thickening by nuclear magnetic resonance imaging with tissue tagging: correlation with sonomicrometers in normal and ischemic myocardium. *J Am Coll Cardiol* (1993) 21:1741–51. doi:10.1016/0735-1097(93)90397-J
48. Forbat SM, Karwatowski SP, Gatehouse PD, Firmin DN, Longmore DB, Underwood SR. Rapid measurement of left ventricular mass by spin echo magnetic resonance imaging. *Br J Radiol* (1994) 67:86–90. doi:10.1259/0007-1285-67-793-86
49. Aurigemma G, Davidoff A, Silver K, Boehmer J, Pattison N. Left ventricular mass quantitation using single-phase cardiac magnetic resonance imaging. *Am J Cardiol* (1992) 70:259–62. doi:10.1016/0002-9149(92)91285-C
50. Solano JP, Gomes B, Higginson IJ. A comparison of symptom prevalence in far advanced cancer, AIDS, heart disease, chronic obstructive pulmonary disease and renal disease. *J Pain Symptom Manage* (2006) 31:58–69. doi:10.1016/j.jpainsymman.2005.06.007
51. Piechnik S, Ferreira V, Lewandowski A, Ntusi NA, Banerjee R, Holloway C, et al. Normal variation of magnetic resonance T1 relaxation times in the human population at 1.5 T using ShMOLLI. *J Cardiovasc Magn Reson* (2013) 15:13. doi:10.1186/1532-429X-15-13
52. Piechnik SK, Ferreira VM, Dall'Armellina E, Cochlin LE, Greiser A, Neubauer S, et al. Shortened Modified Look-Locker Inversion recovery (ShMOLLI) for clinical myocardial T1-mapping at 1.5 and 3 T within a 9 heartbeat breathhold. *J Cardiovasc Magn Reson* (2010) 12:69. doi:10.1186/1532-429X-12-69
53. Ferreira V, Piechnik S, Dall'Armellina E, Karamitsos TD, Francis JM, Choudhury RP, et al. Non-contrast T1-mapping detects acute myocardial edema with high diagnostic accuracy: a comparison to T2-weighted cardiovascular magnetic resonance. *J Cardiovasc Magn Reson* (2012) 14:42. doi:10.1186/1532-429X-14-42
54. Cameron IL, Ord VA, Fullerton GD. Characterization of proton NMR relaxation times in normal and pathological tissues by correlation with other tissue parameters. *Magn Reson Imaging* (1984) 2:97–106. doi:10.1016/0730-725X(84)90063-8
55. Puntmann VO, Voigt T, Chen Z, Mayr M, Karim R, Rhode K, et al. Native T1 mapping in differentiation of normal myocardium from diffuse disease in hypertrophic and dilated cardiomyopathy. *JACC: Cardiovascular Imaging* (2013) 6:475–84. doi:10.1016/j.jcmg.2012.08.019
56. Wacker CM, Bock M, Hartlep AW, Beck G, van Kaick G, Ertl G, et al. Changes in myocardial oxygenation and perfusion under pharmacological stress with dipyridamole: assessment using T\*2 and T1 measurements. *Magn Reson Med* (1999) 41:686–95. doi:10.1002/(SICI)1522-2594(199904)41:4<686::AID-MRM6>3.3.CO;2-0
57. Sebastian J, Flacke SEF, Christine H. Lorenz measurement of the gadopentate dimeglumine partition coefficient in human myocardium in vivo: normal distribution and elevation in acute and chronic infarction. *Radiology* (2001) 218:703–10. doi:10.1148/radiology.218.3.r01fe18703
58. Messroghli DR, Greiser A, Frohlich M, Dietz R, Schulz-Menger J. Optimization and validation of a fully-integrated pulse sequence for modified Look-Locker inversion-recovery (MOLLI) T1 mapping of the heart. *J Magn Reson Imaging* (2007) 26:1081–6. doi:10.1002/jmri.21119
59. Sparrow P, Messroghli DR, Reid S, Ridgway SP, Bainbridge G, Sivanthanthan MU. Myocardial T1 mapping for detection of left ventricular myocardial fibrosis in chronic aortic regurgitation: pilot study. *AJR Am J Roentgenol* (2006) 187:630–5. doi:10.2214/AJR.05.1264
60. Li D, Dhawale P, Rubin PJ, Haacke EM, Gropler RJ. Myocardial signal response to dipyridamole and dobutamine: demonstration of the BOLD effect using a double-echo gradient-echo sequence. *Magn Reson Med* (1996) 36:16–20. doi:10.1002/mrm.1910360105
61. Reeder SB, Faranesh AZ, Boxerman JL, McVeigh ER. In vivo measurement of T2 star and field inhomogeneity maps in the human heart at 1.5 T. *Magn Reson Med* (1998) 39:988–98. doi:10.1002/mrm.1910390617
62. Anderson LJ, Holden S, Davis B, Prescott E, Charrier CC, Bunce NH, et al. Cardiovascular T2-star (T2\*) magnetic resonance for the early diagnosis of

- myocardial iron overload. *Eur Heart J* (2001) 22:2171–9. doi:10.1053/ehj.2001.2822
63. Positano V, Pepe A, Santarelli MF, Scattini B, De Marchi D, Ramazzotti A, et al. Standardized T2\* map of normal human heart in vivo to correct T2\* segmental artefacts. *NMR Biomed* (2007) 20:578–90. doi:10.1002/nbm.1121
  64. Messroghli DR, Wassmuth R, Zagrosek A, Rudolph A, Schulz-Menger J. Assessment of myocardial T2\* from pixel-by-pixel maps on a clinical MR system. *J Cardiovasc Magn Reson* (2008) 10(Suppl 1):A240. doi:10.1186/1532-429X-10-S1-A240
  65. Moon JC, Messroghli DR, Kellman P, Piechnik SK, Robson MD, Ugander M, et al. Myocardial T1 mapping and extracellular volume quantification: a Society for Cardiovascular Magnetic Resonance (SCMR) and CMR Working Group of the European Society of Cardiology consensus statement. *J Cardiovasc Magn Reson* (2013) 15:92. doi:10.1186/1532-429X-15-92
  66. Thuny F, Potton L, Rapacchi S, Thibault H, Bergerot C, Viallon M, et al. Myocardial T1-mapping for early detection of left ventricular myocardial fibrosis in systemic sclerosis. *J Cardiovasc Magn Reson* (2011) 13(Suppl 1):M10.
  67. Thibault H, Ernande L, Rapacchi S, Viallon M, Bergerot C, Thuny F, et al. Early detection of myocardial fibrosis in type II diabetic patients using MR T1-mapping. *J Cardiovasc Magn Reson* (2011) 13(Suppl 1):O110. doi:10.1186/1532-429X-13-S1-O110
  68. Ellims AH, Iles LM, Ling LH, Chong B, Macciocca I, Slavin GS, et al. A comprehensive evaluation of myocardial fibrosis in hypertrophic cardiomyopathy with cardiac magnetic resonance imaging: linking genotype with fibrotic phenotype. *Eur Heart J Cardiovasc Imaging* (2014) 15(10):1108–16. doi:10.1093/ehjci/jeu077
  69. Kammerlander AA, Marzluf BA, Zotter-Tufaro C, Aschauer S, Duca F, Bachmann A, et al. T1 mapping by CMR imaging from histological validation to clinical implication. *JACC Cardiovasc Imaging* (2016) 9(1):14–23. doi:10.1016/j.jcmg.2015.11.002
  70. Sibley CT, Noureldin RA, Gai N, Nacif MS, Liu S, Turkbey EB, et al. T1 mapping in cardiomyopathy at cardiac MR: comparison with endomyocardial biopsy. *Radiology* (2012) 265(3):724–32. doi:10.1148/radiol.12112721
  71. Maceira AM, Prasad SK, Hawkins PN, Roughton M, Pennell DJ. Cardiovascular magnetic resonance and prognosis in cardiac amyloidosis. *J Cardiovasc Magn Reson* (2008) 10:54. doi:10.1186/1532-429X-10-54
- Conflict of Interest Statement:** The authors declare that the research was conducted in the absence of any commercial or financial relationships that could be construed as a potential conflict of interest.
- Copyright © 2017 Hamilton-Craig, Strudwick and Galloway. This is an open-access article distributed under the terms of the Creative Commons Attribution License (CC BY). The use, distribution or reproduction in other forums is permitted, provided the original author(s) or licensor are credited and that the original publication in this journal is cited, in accordance with accepted academic practice. No use, distribution or reproduction is permitted which does not comply with these terms.